Accelerating Yield Mapping at Low Data Rates using Compressive Field Estimate

Thomas Hänel and Nils Aschenbruck

University of Osnabrück
Institute of Computer Science
Wachsbleiche 27, 49090 Osnabrück, Germany
{haenel & aschenbruck}@uos.de

***Abstract*—Increasing the efficiency of farming has been one of, if not the, most important factor in human development since the neolithic age. It laid the path for mankind's accomplishments in the present age. Even today, new improvements are required. One of the most promising improvements is precision farming which demands a spatial distribution of crop parameters in order to cultivate plants in every location in precisely the correct way, e.g. by supplying the perfect amount of fertilizer. One convenient way to gain such a distribution is measuring data on a combine harvester while driving across the field. When data is simply collected on board and transferred and evaluated later, huge amounts of data may be collected. However, being able to estimate the distribution while being on the field has some promising advantages ranging from getting improved status information or satisfying the curiosity of farmers to being able to predict when the harvester needs to empty its tank. The major challenge in transmitting the data is having only access to low bandwidth links due to underdeveloped public land mobile network infrastructures in rural areas. We propose Compressive Field Estimate (CFE), an approach for sending compressed data on the go in order to gain an early estimate of the whole spatial scalar field of plant and ground parameters. Lastly, we demonstrate CFE's performance in a simulative evaluation based on a trace recorded by a harvester on a spacious field.**

***Index Terms*—Precision Farming, Compressive Sensing, Yield Mapping**

I. Introduction

A key contribution to increasing the efficiency of agriculture lies in the cultivation of larger fields with less manpower. To achieve this, more complex farming machinery and even partially autonomous vehicles are required. This leads to the desire to locally or even remotely control and monitor both the progress of harvest as well as the condition of machines. A major challenge arises from transmitting the collected data. The usage of satellite communication networks is usually too expensive and data rates are rather low. Building the infrastructure for local networks, such as WiFi, is also too expensive due to the huge areas. The remaining networks are public land mobile networks. However, rural areas are usually somewhat neglected by providers as the population density and thereby the number of potential customers is too low. For example in rural areas in Europe, often only 2G is available. Low signal quality and loss of connection lead to a further reduced average bandwidth.

We concentrate on the sensor data that describes spatial distributions such as crop yield and crop humidity and propose an approach for compressing and transmitting the data while collecting it. We call the approach Compressive Field Estimate (CFE) as it is based on compressive sensing and allows for estimating the whole scalar field from few measurements. The number of measurements is limited by the available bandwidth.

The remainder of the paper is structured as follows: in section II we give an overview of related work leading to the description of our approach CFE in section III. Afterwards, we apply CFE to an extensive trace of crop yield data recorded by a combine harvester. This is divided into the following steps: firstly, we describe the preprocessing steps of the data in section IV. In section V we analyze the suitability of the data for CFE to find an appropriate parametrization for the performance evaluation in section VI and the comparison against other approaches in section VII. Finally, we draw a conclusion in section VIII.

II. Related Work

A. Precision Farming

Around the beginning of the new millennium, the concept of precision farming, also known as precision agriculture, was pushed forward [1], [22]: Its main idea is changing cultivation of small areas individually. This encompasses mainly supplying precisely the correct amount of fertilizer and irrigation in each area. As this allows for getting maximal yield at minimal use of fertilizers, it promises more efficient and sustainable farming even on huge fields. A crucial preparation step for this is gaining information on the spatial fields of various parameters that allow for estimating the required amount of fertilizer. A lot of research has been spent on gaining these spatial fields based on satellite- or aircraft-based remote sensing [16]. Newly explored alternatives are for example wireless sensor networks [2], [17]. Mapping from the sensed parameters to the most interesting spatial field, the crop yield, still is a cumbersome task. Thus, measuring the yield while harvesting, which was established even before the rise of precision farming [3], remains an essential element of precision farming. Besides the above mentioned benefits, there are certain applications that profit from getting the data

DOI 10.1109/LCN.2017.56

during harvest rather than afterwards. Firstly, the owner of the field may want to monitor the progress of harvest. Secondly, the data may be used to predict trading prices [18] and it is desirable to know these prices as early as possible. Thirdly, transport vehicles which collect the crop from the harvester need to be exchanged whenever one is full. Predicting the time and location of these exchanges based on the current yield rate allows for a more efficient navigation of the transport vehicles. Nevertheless, yield mapping has drifted out of research focus in the meanwhile. We believe, it's time to revisit the topic applying new technologies that have been developed in the meanwhile such as Compressive Sensing (CS).

B. Compressive Sensing

Compressive Sensing (CS) is a relatively new concept [5] that allows for compressing data while measuring. It has been prominently described by Candes et al. [4]. For a short summary of CS, let us assume the task of measuring and transmitting or storing a vector x of size N. With CS, the measurement process is changed to instead measure or calculate the vector $y = \Phi x$ of size M with $M << N$ and Φ being an $M \times N$ matrix that describes the measurement. From this compressed vector y, x may be reconstructed assuming that there is some known linear transformation in which x may be represented sparse, i.e. with few zeros:

$$x = \Psi f \tag{1}$$

where f denotes the transformed vector and Ψ the transform matrix. Common examples for such a transform are Discrete Cosine Transform (DCT), Discrete Fourier Transform (DFT), and Discrete Wavelet Transform (DWT). The equation to solve is:

$$f_{estimate} = \underset{f}{\operatorname{argmin}} ||f||_0 \text{ with } y \approx \Phi\Psi f \tag{2}$$

Where the '$\approx$' sign pays respect to the fact that the constraint will usually not be exactly fulfilled due to noisiness of the data. The result may be put into equation (1) in order to gain an estimate for x. Apart from x being sparse in some transform, Φ needs to be incoherent with Ψ which is the case at surprisingly high probability when using a random matrix for Φ. As shown by [19], in many cases Φ may even be sparse which translates into choosing a subset of samples from x for y. This special case allows for sub-Nyquist sampling, as due to the irregularity of sampling, x may be reconstructed even if the resulting mean sampling rate used for building y is lower than requested by the Shannon-Nyquist theorem [4].

C. Measuring Scalar Fields with CS

In the beginning, the exploitation of sub-Nyquist sampling made time series an obvious field of research. But researchers soon expanded their considerations to the measurement or sensing of two-dimensional scalar fields. Whereas these scalar fields are usually camera images [20] or medical imagery [14], environmental monitoring with static wireless sensor networks attracted some interest as well [13], [7]. However, the CS-based measurement of an environmental scalar field with moving devices has only been rarely considered and usually a rather high number of devices, which are homogeneously distributed, is considered [21], [11]. In contrast to this we pay attention to a – to the best of our knowledge – previously not examined aspect: When exploring a new area with few devices or even just one, the available information is focused only on a small, slowly increasing subset of the area. Therefore, our proposed approach CFE performs not only a compression but also a forecast for the still unexplored area. Alternatively, in conjunction with the sparse sampling mentioned in section II-B, the compression may instead be seen as an interpolation, similarly to the considerations in [21] and consequently the forecast as an extrapolation.

In the robotics community, scalar field estimation has been explored as well (e.g., [9]). However, they heavily rely on navigating a robot for maximal information gain. In real-world applications this is often undesirable as movement is predetermined by the main task whereas sensing is just a side task.

III. The Idea behind Compressive Field Estimate (CFE)

To quickly sum up the challenge we consider, we have a harvester that is harvesting a crop field and measures various information with some of this information being spatially distributed scalar fields. Some remote operator is interested in gaining the whole scalar field. Classic approaches to transmit the data encompass transmitting measured values in order as fast as possible or collecting the data and transmitting it in the end in compressed form. The former approach is usually preferable as it allows for a live preview.

However, imagine the case that the time τ to transmit a sample is longer than the time δ between measuring two consecutive samples. Then, the transmitted values quickly lack behind as the data rate is too low. Not even emerging technologies such as 5G and LoRa aim to combine high data rates with good coverage in rural areas: 5G concentrates on higher data rates in small and dense cells [8] which is more suited for urban areas whereas LoRa [12] concentrates on offering long ranges suitable for rural areas but it offers low data rates. We expect this problem to persist in the future as improving public land mobile networks infrastructure in rural areas will remain unattractive for wireless providers due to low population densities. Furthermore, harvesters acquire more and more information at increasing rates, so that only a small portion of the available bandwidth may be used for each scalar field.

We propose CFE as a new approach that builds upon the toolkit of CS to send and recover data in a way that allows for a faster recovery of the whole scalar field. The core principle is to not simply send samples in order but rather selecting samples for transmitting randomly from the values measured so far. To put it more formally, the harvester begins measuring at t_0, taking a measurement every δ seconds. The sample measured at time t is called x_t The corresponding coordinates (either geographical or indexes in a grid) are called i_t and j_t

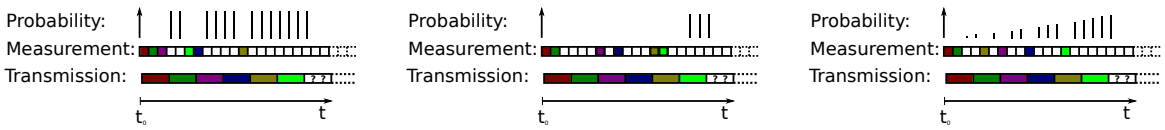

(a) $CFE_{uniform}$ **(b)** CFE_{latest} **(c)** CFE_{ramp}

Fig. 1: Examples and probability densities for different sampling strategies.

. At time T_{now} the harvester has all tuples $(x_{t'}, i_{t'}, j_{t'})$ with $t' \leq t$ in its storage. It sends tuples every τ seconds randomly selected from the available samples. So that at time t there are $(t-t_0)/\delta$ samples in the harvesters storage and $(t-t_0)/\tau$ samples in the storage of the remote evaluation center.

This randomization is the only change required at the harvester. The compressive sensing toolkit is applied at the remote evaluation center. Instead of a time series representation, it uses a spatial representation. For now, let us assume that some preprocessing assures that we get at most one measurement per location and the locations form a two-dimensional grid. With every received tuple we can fill in one cell in the grid: $x_{i,j}$ with $0 \leq i < I$ and $0 \leq j < J$. The total number of grid cells is $N = I \cdot J$. For CS, a vector representation is more desirable, therefore, we introduce a new index $l = i \cdot J + j$ that allows addressing all cells of the grid. The vector of all x_l is called x.

The task of the remote evaluation center is recovering x from the measured x_l. The vector of all measured x_l at time t is called y_t and has length $M_t = (t - t_0)/\tau$. Note that the extraction of y_t from the unknown vector x may be represented with a matrix product: $y_t = \Phi_t x$ where Φ_t is an $M_t \times N$-matrix in which all $\phi_{l',l}$ are set to one where l denotes a received packet in x and l' the same element in y_t. All other elements of Φ are set to zero. So with every received measurement, a new row is appended to the matrix, which results in an identity matrix where random rows have been removed. With this measurement matrix and the vector of received measurements y_t, the remote evaluation center has a common CS-problem to solve (compare equation (2)):

$$f_{estimate,t} = \underset{f}{\operatorname{argmin}} ||f||_0 \text{ with } (y_t - \bar{y}_t) \approx \Phi_t \cdot \Psi \cdot f \quad (3)$$

Where Ψ now denotes the matrix of the two-dimensional transform which may be constructed from the corresponding matrix of the one-dimensional transform using the Kronecker product [6]. The mean of the measurements $\bar{y}_t$ has been removed as solvers struggle with the reconstruction of the offset. From $f_{estimate,t}$ an estimate for x may be calculated:

$$x_{estimate,t} = \Psi \cdot f_{estimate,t} + \bar{y}_t \quad (4)$$

Note that the compression ratio R decreases over time:

$$R(t) = \frac{F}{M_t} = \frac{\tau \cdot F}{(t - t_0)} \quad (5)$$

Where F denotes the amount of cells in the grid that are actually part of the field. This naturally leads to an increase of reconstruction quality. At $t_e = \tau \cdot F + t_0$ all samples have been received. Therefore, the compression ratio has decreased to $R(t_e) = 1$ and the reconstruction is perfect as the constraint in equation (3) allows only a single solution. However, the normal way would be to abort the transmission earlier, once a sufficient compression ratio has been reached and thereby a lossy compression has been performed.

A. Random sampling strategy

So far, we have omitted one question on the harvester side: which strategy is used for the selection of values to transmit? At $t_p = F \cdot \delta + t_0$ the harvester has explored the whole area. From here on it may select values from its storage uniformly that have not been transmitted yet. Before t_p, an adequate strategy is required. There are two straight forward approaches: In the first approach (Fig. 1a), samples are selected uniformly from the un-transmitted values in storage at all times. Therefore, we call it $CFE_{uniform}$. In the second approach (Fig. 1b), the sample is selected only from samples that have been measured since the last transmission, i.e. all $x_{t'}$ with $t - \tau < t' \leq t$. We call this approach CFE_{latest}.

$CFE_{uniform}$ may lead to poor reconstruction quality as more samples will be selected from the beginning of the measurement leading to a non-uniform distribution over the whole field. A potential problem that may arise when using CFE_{latest} is that the selected values may be a checkerboard-like pattern, only distorted by some jitter. Such a checkerboard pattern is periodic and, therefore, coherent with common transform matrices such as DCT and DFT which leads too poor reconstruction quality [4]. In order to further explore this trade-off we try a third strategy (Fig. 1c) with a probability density that is increasing linearly over the un-transmitted samples in a timely order. Due to the form of the probability density function we call this approach CFE_{ramp}. In figure 1c the ramp seems distorted due to the samples which have been transmitted already. Showing only the un-transmitted samples, the ramp would be perfectly linear. The extension to other monotonically increasing probability density functions may be a promising improvement for future work.

B. Remarks

We would like to make some remarks about the benefits of our approach that go beyond what is covered in the following evaluations: The change of transmissions only affects the order and not the content of the measurements, so each single transmission keeps a meaning on its own. Building the measurement matrix from the received samples has two

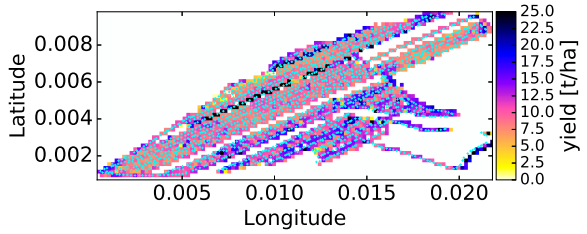

Fig. 2: The location of samples and the resulting grid distribution for the crop yield.

key benefits. Firstly, no additional information, such as the seed for generating the measurement matrix [21], needs to be exchanged and secondly it does not need to be known which data has been sent originally. The latter can be exploited in multiple ways: If only an approximate field is required, transmissions may be simply stopped earlier. Dealing with lost packets is particularly easy as pointed out by [7] and others: If a lossy reconstruction suffices, no explicit retransmit is required - transmission goes on until sufficient packets have been received. If a full reconstruction is desired, some form of Automatic Repeat reQuest (ARQ) mechanism may be used. As duplicate packets or a wrong order of packets do not influence the reconstruction, CFE is very insensitive towards the ARQ system in use. For the estimate just like for the lossy reconstruction, packet loss only leads to a more slowly increasing reconstruction quality.

A special case arises when the harvester crosses areas that have been explored before or stops for some time: as no relevant new values are measured, CFE_{latest} has to select values uniformly instead. The other strategies may proceed as before. This situation presents a relaxation of the problem as the gap between measurement rate and transmission rate is reduced. Therefore, in this paper, we focus on the worst case scenario with no stops.

IV. Preprocessing

Before we can actually evaluate CFE's performance, some preprocessing is required. The evaluations in the following sections are based on traces from a harvester working on a field in an area of approximately $1.7\,\mathrm{km}$ by $0.5\,\mathrm{km}$. The harvester collected telemetry data every five seconds. We concentrate on data that describes spatial distributions across the field, namely the yield and the humidity of the crop. As most spatial compression algorithms concentrate on data in a grid, we build such a grid in a preprocessing step as follows: First an empty grid is initialized with a fixed cell size. Then, we iterate the trace of samples in the order of recording. For each sample the corresponding grid cell is determined. If the grid cell is empty and the value of the sample is not zero, the value of the sample is assigned to the grid cell. Otherwise, the sample is ignored. Our motivation for this approach rather than using the sum or mean of the values is the following line of thought: If the value is zero, either the harvester is currently not harvesting or the area has already been cleared. In both cases, the values do not reflect the original spatial distribution. We only consider the first value as when harvesting in a grid cell, the spatial distribution is disturbed, making later measurements incorrect.

While creating the grid, a new trace is generated that only contains samples contributing to the grid and replaces the original trace in the following evaluations. This trace contains some unnatural movement as there are jumps when the harvester crosses already explored areas. However, a more natural trace makes the evaluation less expressive as a lot of data can be transmitted during breaks and while crossing already explored areas. Thereby, the generated trace represents the worst case scenario as discussed in section III-B.

After preprocessing, the conditions described in section III are fulfilled. When using the approach in reality, this preprocessing may be either performed on the harvester or in a remote evaluation center. The only prerequisite is the desired grid size which may be set based on the field shape calculated in previous years (e.g. using the algorithm from [10]).

Figure 2 shows the locations of the original measurements and the resulting grid. The coordinates have been anonymized by removing an offset in order to preserve the privacy of the owner. Note that we have chosen the grid cell size as a trade-off being coarse enough to avoid gaps in the distribution and fine enough to not waste too many of the original samples. The displayed distribution is the one of the crop yield, i.e. the amount of crop that was collected per area in tons per hectare (t/ha).

V. Data Suitability

In order to apply CS and thereby CFE to the data, three conditions must be met, (1) the data needs to be sparse in some domain, (2) a suitable measurement process must be applied, and (3) the measurement and the transformation from the sparse domain must be incoherent. The second condition, the existence of a measurement process, was already explained in section III. For an examination of the first condition, the sparsity, we applied multiple common transformations to the grid data, namely DCT, DFT, and the Haar transform as a representative for DWTs. Furthermore, we considered the untransformed version. As we are focusing on spatial distributions, we used the two-dimensional versions of the transforms.

Figure 3a shows the resulting coefficients in descending order. For comparability, they were scaled so that the maximal value is one. In the untransformed case (*Spike*) the magnitude of the highest approximately 1800 values decreases slowly. Then there is a sudden drop from 0.17 to 0 with all remaining values being zero. The zero values are simply those outside the measurement area whereas the non-zero values are those within the measurement area of size $f = 1782$. This border is depicted as a dashed line. The coefficients in Haar domain decrease about as slowly as the untransformed values. The sudden drop is missing, instead the trend is held across all values. The coefficients in frequency domain display a significantly steeper decrease. Only 97 values have a magnitude larger than 0.05 in DFT. For DCT there are only 25 values. After

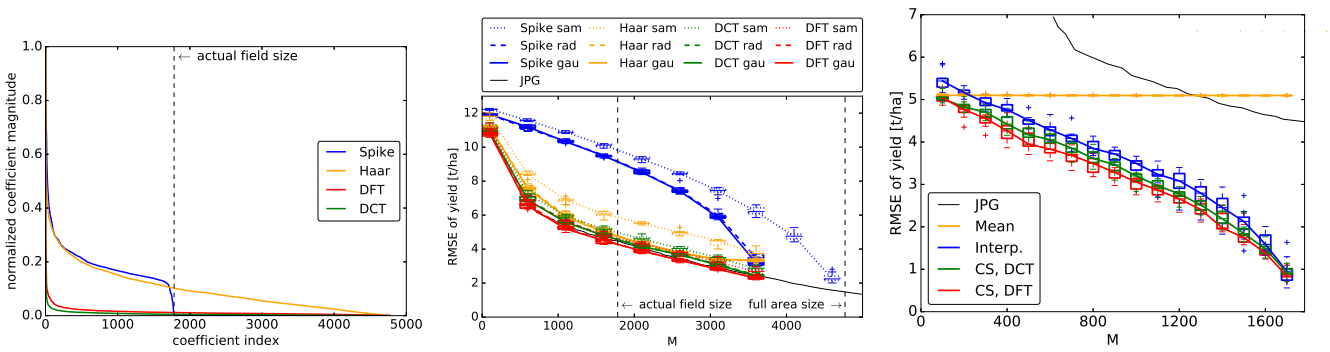

(a) Coefficients in various domains in descending order.

(b) Reconstruction quality for various pairs of Ψ and Φ.

(c) Samples extracted solely from the relevant area.

Fig. 3: Examining the suitability of the data for CS and CFE.

all, especially the two frequency space transformations DFT and DCT are promising candidates to be used in compressive sensing.

To further restrict our selection of Ψ and Φ, we compressed and decompressed the grid data using the compressive sensing scheme with all combinations of the transform matrices Identity (*Spike*), Haar, DCT, and DFT and the measurement matrices Identity (*sam*), Rademacher (*rad*), and Gaussian (*gau*). Implicitly, this also contains a test of the third condition, the incoherence. We used the solver SL0 [15] as it gives a good compromise of speed and reconstruction quality in our experience, is easy to implement, and supports complex values and thereby DFT. A comparison of solvers lies outside the scope of this paper. As a metric for the quality of the reconstruction we use the Root Mean Square Error (RMSE) between the original and the reconstructed field. This evaluation is limited to the area where we actually have measurements. The results are shown in figure 3b where the boxplots are based on random measurement matrices generated from ten different seeds. For comparison, the reconstruction quality of JPEG is shown as well, being one of the most established compression algorithms for two-dimensional fields. For JPEG we scaled the measured values to the range of a byte. Due to this byte-wise representation, the file size in byte is a metric that is approximately equivalent to M. Therefore, we use it as M in the evaluation.

The RMSE of the compressive sensing results with DCT, DFT, and Haar transform is about as low as the one for JPEG and shows the same continuous decrease in dependence of M. In a stark contrast, the RMSE for the untransformed case (*Spike*) is significantly higher and decreases slower up to an M-value of approximately 3000. Then, the decrease becomes steeper. This change may be attributed to the fact that from here on M is sufficiently higher than the approximately 1700 non-zero values due to the limited measurement area. Whereas there is no significant difference in the RMSE for the Gaussian and Rademacher measurement matrices, the results with random sample matrices fall behind especially in the case of Haar tranform and the untransformed case. For DCT and DFT the difference is rather small due to the incoherence with random sampling which was proven in [19]. The overall disappointing result in comparison with JPEG may be attributed to the waste of samples for reconstructing the values outside the actual measurement area.

However, random samples open up an elegant way for circumventing the problem by just using samples within the measurement area. The result is depicted in figure 3c. Note that the task performed by compressive sensing now resembles an interpolation more than a typical compression. Therefore, we included a linear interpolation between the random values for comparison as well as the most trivial interpolation which is just assuming the mean of the samples for the whole field. For comparability with figure 3b, we again included the result with JPEG compression. As we are using random samples for the measurement, we limited our evaluations to DCT and DFT.

Both, the interpolation techniques as well as compressive sensing, yield drastically better results than JPEG because JPEG still suffers from wasting data on the area outside of the field as well as having some more overhead. In contrast to all other techniques, the mean has a constant RMSE of approximately $5\,\mathrm{t/ha}$ and barely shows any improvements with an increasing number of samples. Linear interpolation and CS use the mean as default value and improve upon it. Therefore, they become better than the mean assumption even with a small number of samples. CS with DCT shows results that are slightly better than with linear interpolation. Using DFT, the difference gets even clearer, significantly less samples are required for the same reconstruction quality. Note, that this is already a significant result for certain applications: measurements of the mass of plants that may be harvested can be taken at some random locations on the field in order to get an estimate for the yield distribution.

VI. Performance of CFE

Having shown the achievable performance when sampling from the whole field area in section V which we refer to as

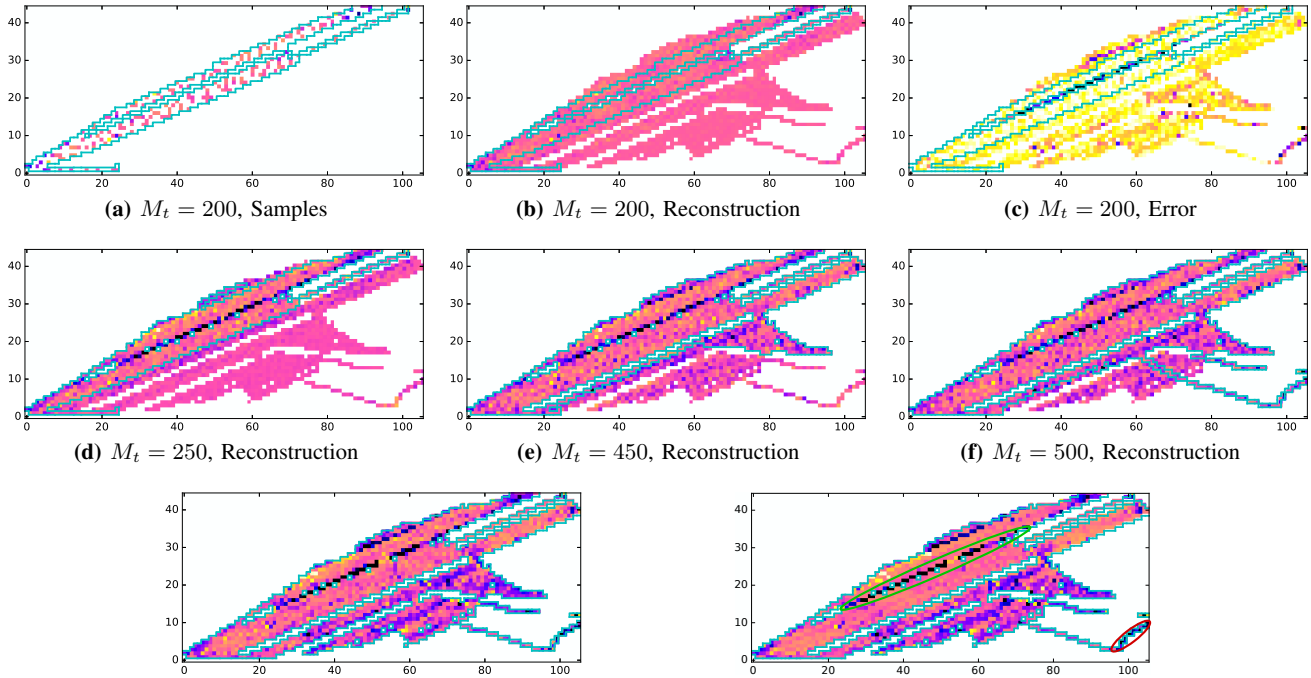

(a) $M_t = 200$, Samples **(b)** $M_t = 200$, Reconstruction **(c)** $M_t = 200$, Error

(d) $M_t = 250$, Reconstruction **(e)** $M_t = 450$, Reconstruction **(f)** $M_t = 500$, Reconstruction

(g) $M_t = 1200$, Reconstruction **(h)** $M_t = 1780$, Reconstruction

Fig. 4: Development of the reconstruction quality during harvest.

the static case from here on, we now consider the case of transmitting samples while driving and, therefore, not having all values available using CFE as proposed in section III. This approach will be called CFE or the dynamic case from here on. As discussed in section III, we applied the three different strategies for selecting samples for transmission in the dynamic case. The limited bandwidth is simulated by being able to transmit only one sample every $\tau = 15\,\mathrm{s}$ while measuring a sample every $\delta = 5\,\mathrm{s}$, which are values typically used for low- and high-rate sampling.

A. Qualitative evaluation

In order to gain an intuition for CFE's performance, we first compare its performance at different points of time and thereby a different number of received samples. For now, we limit our considerations to the sampling strategy CFE_{latest}. The samples that have been transmitted as well as the results after reconstructing the field solving equations (3) and (4) are shown in figure 4. Note that in favor of a more compact visualization, we have omitted the color bar and changed to integer indexes for the grid cells rather than longitude and latitude. This information may be obtained from figure 2.

The first row (Fig. 4a–c) shows the situation after having received the first $M_t = 200$ samples. Figure 4a shows the samples that have been received. The borderline of the area which has been explored by the harvester at this time is shown for comparison. The samples display a homogeneous distribution within the explored area due to the sampling strategy CFE_{latest}. In figure 4b, the reconstruction result is shown.

Note, that we have set all cells outside the field to 0 as this area has no relevance and would be rather distracting. In the areas far from the explored area, the values default to the mean due to its temporary removal in equations (3) and (4) and display relatively high deviations (Fig. 4c). In the explored area, the distribution already has some similarity to the original distribution (see figure 2 or 4h for comparison). In the upper left of the field there is a row with high deviations. The original distribution reveals that it coincides with a row of higher yields highlighted by a green ellipse in figure 4h. Shortly after, when $M_t = 250$ readings have been received (Fig. 4d), this row has been crossed by the harvester and seems to be well captured in the reconstruction (Fig. 4d) but there are still some errors along this row. After $M_t = 450$ readings (Fig. 4e), diagonal stripes which coincide with the movement pattern of the harvester become apparent in the reconstruction. This is actually a step in the right direction when comparing with the real distribution in figure 4h which also contains such stripes. This structure was forced by the assumed DFT which demonstrates an explanation for DCT's and DFT's superiority determined in section V. After $M_t = 500$ (Fig. 4f), nearly the whole area has been explored by the harvester. Afterwards (Fig. 4g), the reconstruction gradually improves by filling the gaps with more values, getting very close to the original (Fig. 4h) and ultimately identical to it after transmitting all values.

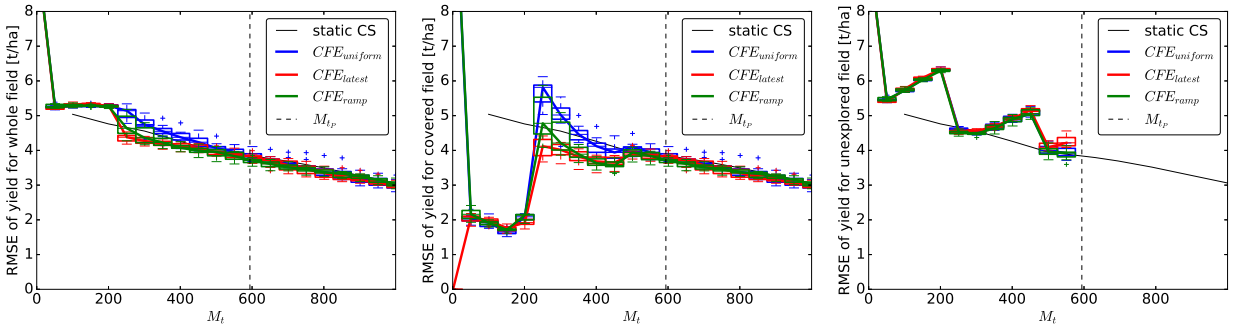

(a) Estimate of whole field.

(b) Estimate of explored part of field.

(c) Forecast for unexplored part.

Fig. 5: Reconstruction quality in the dynamic case with different sampling strategies and metrics.

B. CFE as field estimate

Although the distributions in figure 4 provide a more detailed understanding, this is not suitable for a broader evaluation. Instead we again measure the quality of the field estimate using RMSE as in section V, this time for the dynamic case. Therefore, the M_t axis now also serves as a time axis. The results are shown in figure 5a. The behavior may be roughly separated in two phases: in the first phase the harvester did not explore the whole field. Here the reconstruction is a mixture of compression and forecast. The change between phases occurs at $t_P = t_0 + F \cdot \delta$ or after receiving $M_{t_P} = t_P/\tau = 594$ samples. Initially, all dynamic sampling strategies perform worse than the static case. The RMSE decreases with increasing M_t for the dynamic as well as the static case. However, the decrease is less regular but overall steeper in the dynamic case. Even before t_P, all strategies achieve RMSEs about as low as in the static case. This is actually a remarkable result as it shows that the influence of the restricted sampling is so insignificant for the whole field that it disappears even before having covered the whole field. The results also help us finding the appropriate sampling strategy: Mostly, the reconstruction quality is not significantly different. However, in the phases where it is different, the result is somewhat surprising considering the trade-off discussion from section III-A: CFE_{latest} is a clear winner. It continuously shows better results than the other strategies with $CFE_{uniform}$ coming in last and CFE_{ramp} in between the two. We attribute the superiority of CFE_{latest} to the fact that the achieved homogeneous distribution of samples dominates the reconstruction quality whereas the resulting measurement pattern does not become less incoherent with the transformation base because sufficient randomization is induced by the route of the harvester as well as the jitter.

The first phase requires some more investigation in order to separate the influence of compression and forecast.

C. CFE as compression

First we evaluate the influence of the compression area by calculating the RMSE only for the part of the area that has been explored by the harvester already. The result is shown in figure 5b. As expected, in the beginning, the overall RMSE is mostly lower than for the whole field estimate (Fig. 5a). Note that from M_{t_P} onwards, the values are the same as in figure 5a because the area that contributes to the RMSE calculation becomes the same in phase two.

The ranking of the sampling strategies is the same as for the whole field estimate. At the beginning when only few values from a highly localized area have been transmitted, the RMSE is highly volatile. Whereas this may be partially attributed to the small sample size of grid cells, the course is qualitatively the same for all random seeds and sampling strategies, indicating that it is mainly influenced by the real data of the field and the exploration path. When comparing with figure 4, e.g., the steep increase between $M_t = 200$ and $M_t = 250$ may be explained: The row of high yield values in the upper left area of the field has been harvested in between these points of time as a comparison of figures 4b and 4d reveals. In several cells, reconstruction errors were made around this row, generating the steep increase. The difference between the strategies which is observable in figure 5a as well, is most significant during and after this increase.

D. CFE as forecast

In the next step, we take a look at the reconstruction quality in the unexplored area. This is shown in figure 5c. Naturally, this evaluation can only be performed up to t_P as there is no unexplored area left afterwards. The RMSE is significantly higher, indicating that the forecast is not very good. The difference between the strategies coincides with the previous observations. Most promising are the drastic improvements of reconstruction quality between $M_t = 200$ and $M_t = 250$ as well as the one between $M_t = 400$ and $M_t = 450$. Comparing with the compression performance, the first increase clearly coincides with the steep decrease of reconstruction quality in figure 5b, indicating that a difficult to reconstruct area has been shifted from unknown to known space, the row of high yields discussed for the compression performance. The same occurs between $M_t = 400$ and $M_t = 450$: The difficult area here

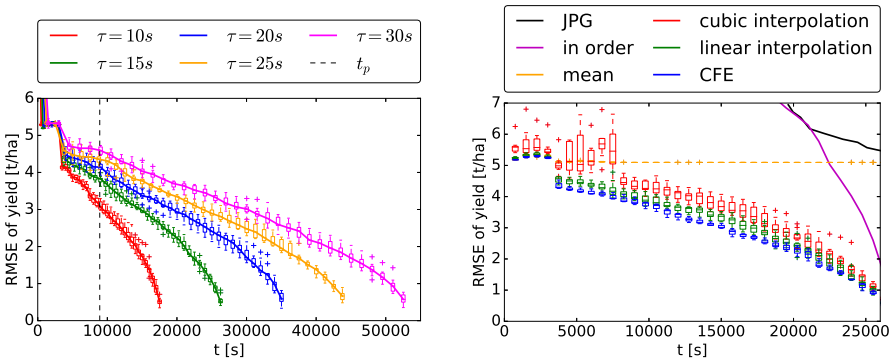

(a) Comparison of bandwidths. **(b)** Comparison with alternatives.

Fig. 6: Reconstruction quality over time.

has been the narrow path in the lower right corner. Figure 4f reveals that the values haven been drastically underestimated in comparison with those in the real distribution which is marked by a red ellipse in figure 4h. In the beginning and in between, the reconstruction quality slowly increases, as the unexplored area decreases and therefore the relatively small difficult areas contribute more to the RMSE.

VII. Timeliness of Results in Comparison

In the previous sections, we mainly used the number of transmitted values M_t in order to compare algorithms, which is a perfectly suited metric for compression performance. However, the availability of data depends on the time and, therefore, we evaluate reconstruction quality over time. This allows us to evaluate the influence of the bandwidth. Thereby, we can assess the situation of having only a limited bandwidth available which we assume to be the usual case. Note that we mainly aim for making good use of a given limited bandwidth rather than trying to save bandwidth. However, one may instead put a lower limit to enforce bandwidth savings. We varied τ, which is directly linked to the available bandwidth b with $b = \gamma/\tau$ where γ is the size of a transmitted tuple. The resulting RMSE over time is shown in figure 6a. The decrease of the RMSE is stretched further over time the lower the bandwidth. An additional effect from the availability of the information for transmission is not observable and thereby negligible.

Taking the timeliness into consideration also allows to expand our considerations to more algorithms. The result is shown in figure 6b: The most basic approach is sending data in the order of measurement, however this leads to a very slow decrease of the RMSE. In order to perform a JPEG-compression, first all data needs to be known. Therefore, it cannot be done before t_p. Assuming that compression can be performed nearly instantly, the time of the completed reception as well as the reception quality depend on the selected quality. Therefore, the line for JPEG in figure 6b has a slightly different meaning: for all other approaches, the reconstruction quality decreases over time. In contrast, for JPEG, just one point on the line is chosen via the quality level.

The approaches that send current data on the go yield better reconstruction quality earlier. Even the rather simple approach of simply predicting the mean of the collected samples for the whole area easily outperforms *in order* and *JPEG* for a long time. The remaining approaches are based on the data transmission scheme of CFE. As it turned out to be the best, we limit our considerations to the strategy CFE_{latest} here. Like in the static case, we choose interpolation techniques for comparison. During interpolation, we again default to the mean of the measured samples outside the convex hull of samples. We have used the two common interpolation methods *linear* and *cubic*. Whereas *cubic* tends to overshoot and, therefore, offers highly volatile reconstruction quality especially in the beginning, *linear* interpolation leads to relatively good reconstruction qualities at all times. CFE is superior for a long time range. Only at the beginning and in the end, linear interpolation can keep up.

VIII. Conclusion & Future Work

We presented CFE, a new approach for transmitting samples of a scalar field during exploration to get a faster estimate of the whole field at limited bandwidth. CFE proved to be successful for crop yield mapping, as the stripe pattern caused by harvester movements may be exploited assuming sparsity in frequency space. We showed that it is insensitive to the selection of samples due to the randomness of the movement, slightly preferring a homogeneous distribution of samples.

In our future work we will take a closer look at short-term forecast performance and expand our approach to other scenarios such as different example fields and different data from other sensors. Furthermore, we will consider less reliable links.

Acknowledgements

We would like to thank the company CLAAS for supplying us with the telematics data. This work was supported by the

”Stifterverband für die Deutsche Wissenschaft” (H170 5701 5020 20951).

REFERENCES

[1] H. Auernhammer, “Precision farming — the environmental challenge,” *Computers and Electronics in Agriculture*, vol. 30, no. 13, pp. 31–43, 2001.

[2] J. Bauer, B. Siegmann, T. Jarmer, and N. Aschenbruck, “On the potential of wireless sensor networks for the in-situ assessment of crop leaf area index,” *Computers and Electronics in Agriculture*, vol. 128, pp. 149–159, 2016.

[3] S. J. Birrell, K. A. Sudduth, and S. C. Borgelt, “Comparison of sensors and techniques for crop yield mapping,” *Computers and Electronics in Agriculture*, vol. 14, no. 2, pp. 215–233, 1996.

[4] E. Candes and M. Wakin, “An introduction to compressive sampling,” *IEEE Signal Processing Magazine*, vol. 25, no. 2, pp. 21–30, 2008.

[5] D. L. Donoho, “Compressed sensing,” *IEEE Trans. on Information Theory*, vol. 52, no. 4, pp. 1289–1306, 2006.

[6] M. Duarte and R. Baraniuk, “Kronecker compressive sensing,” *IEEE Trans. on Image Processing*, vol. 21, no. 2, pp. 494–504, 2012.

[7] F. Fazel, M. Fazel, and M. Stojanovic, “Random access compressed sensing for energy-efficient underwater sensor networks,” *IEEE Journal on Selected Areas in Communications*, vol. 29, no. 8, pp. 1660–1670, 2011.

[8] A. Gupta and R. K. Jha, “A Survey of 5G Network: Architecture and Emerging Technologies,” *IEEE Access*, vol. 3, pp. 1206–1232, 2015.

[9] Z. Jin and A. L. Bertozzi, “Environmental boundary tracking and estimation using multiple autonomous vehicles,” in *Proc. of the 46th IEEE Conf. on Decision and Control (CDC)*, 2007, pp. 4918–4923.

[10] J. Lauer, L. Richter, T. Ellersiek, and A. Zipf, “Teleagro+: Analysis framework for agricultural telematics data,” in *Proc. of the 7th ACM SIGSPATIAL Int. Workshop on Computational Transportation Science (IWCTS)*. ACM, 2014, pp. 47–53.

[11] M. Lin, C. Luo, F. Liu, and F. Wu, “Compressive data persistence in large-scale wireless sensor networks,” in *Proc. of the Global Telecommunications Conf. (GLOBECOM)*, 2010.

[12] “LoRaWan — What is it?” White Paper, LoRa Alliance, 2015.

[13] C. Luo, F. Wu, J. Sun, and C. W. Chen, “Compressive data gathering for large-scale wireless sensor networks,” in *Proc. of the 15th Ann. Int. Conf. on Mobile Computing and Networking (MobiCom)*. ACM, 2009, pp. 145–156.

[14] M. Lustig, D. L. Donoho, J. M. Santos, and J. M. Pauly, “Compressed Sensing MRI,” *IEEE Signal Processing Magazine*, vol. 25, no. 2, pp. 72–82, 2008.

[15] H. Mohimani, M. Babaie-Zadeh, and C. Jutten, “A fast approach for overcomplete sparse decomposition based on smoothed ℓ^0 norm,” *IEEE Trans. on Signal Processing*, vol. 57, no. 1, pp. 289–301, 2009.

[16] D. J. Mulla, “Twenty five years of remote sensing in precision agriculture: Key advances and remaining knowledge gaps,” *Biosystems Engineering*, vol. 114, no. 4, pp. 358–371, 2013, special Issue: Sensing Technologies for Sustainable Agriculture.

[17] Y. Qu, Y. Zhu, W. Han, J. Wang, and M. Ma, “Crop leaf area index observations with a wireless sensor network and its potential for validating remote sensing products,” *IEEE Journal of Selected Topics in Applied Earth Observations and Remote Sensing*, vol. 7, no. 2, pp. 431–444, 2014.

[18] F. Rembold, C. Atzberger, I. Savin, and O. Rojas, “Using low resolution satellite imagery for yield prediction and yield anomaly detection,” *Remote Sensing*, vol. 5, no. 4, pp. 1704–1733, 2013.

[19] M. Rudelson and R. Vershynin, “Sparse reconstruction by convex relaxation: Fourier and gaussian measurements,” in *Proc. of th 40th Ann. Conf. on Information Sciences and Systems (CISS)*, 2006, pp. 207–212.

[20] D. Takhar, J. N. Laska, M. B. Wakin, M. F. Duarte, D. Baron, S. Sarvotham, K. F. Kelly, and R. G. Baraniuk, “A new compressive imaging camera architecture using optical-domain compression,” in *Proc. of the SPIE Conf. on Computational Imaging IV*, vol. 6065, 2006.

[21] X. Yu, H. Zhao, L. Zhang, S. Wu, B. Krishnamachari, and V. O. K. Li, “Cooperative sensing and compression in vehicular sensor networks for urban monitoring,” in *Proc. of the IEEE Int. Conf. on Communications (ICC)*, 2010.

[22] N. Zhang, M. Wang, and N. Wang, “Precision agriculturea worldwide overview,” *Computers and Electronics in Agriculture*, vol. 36, no. 23, pp. 113–132, 2002.